Machine Vision for Knot Detection and Location in Chinese Fir Lumber

Min Ji Wei Zhang Guo-fu Wang Xing-liang Diao
Hu Miao Rui Gao

Abstract

In order to be utilized in the design of a wood building, the lumber must pass grade. Machine-vision inspection grading offers higher efficiency and accuracy than traditional manual visual grading. In this paper, a fast and accurate method for identifying defects in large-size structural lumber based on machine vision of Fujian Chinese fir *(Cunninghamia lanceolata* (Lamb.) Hook) constructional lumber (FCF CL) is proposed. Specifically, the grey matrix of the captured images on the surface of the sawn timber is initially scanned and the pixel weights on the edges of the image greyness variables are calculated. A matrix-valued torus was formed by fitting the knot edge profile and analyzing changes in the gradient values at the knot's edge, as well as calculating the directional derivative's rate of change. The knot three-dimensional mapping curves were projected onto the plane to form horizontal rise contours. Observe from the contour map of the whole large-size sawn timber, and extract the positional information of the knot where there is a trough (groove).

The test results show that the rRMSE (Relative Root Mean Square Error) measured at the x axis position of knots is within 0.49 percent; the rRMSE measured at the y axis is 0.35 percent, which has high detection accuracy and meets the production requirements. We also investigated the effect of knots in different positions on the modulus of elasticity and the bending strength of FCF CL, with a view to establishing a link between machine-vision knot detection and mechanical properties of sawn timber in our next work.

The use of wood in construction is a crucial step toward creating a habitable environment. Modern timber constructions have gained popularity throughout developed North America, Europe, and Asia (Hyun et al. 2018, Panagiotis et al 2018). The extensive utilization of wood in building construction has made it imperative for the wood processing industry to improve its technological proficiency, production efficiency, and automation (Devaru and Gopalakrishnan 2020). China has the biggest plantation system in the world, but because of inadequate automatic detection and quality grading of native tree species, the resource-rich plantations cannot be used to produce structural materials for buildings (Ahn et al. 2021). The main component of structure buildings is load-bearing timber. Its mechanical qualities and strength grade have a significant influence on encouraging the use of prefabricated, multi-story timber constructional buildings and are directly tied to the safety of such structures (Chang et al 2018, Park et al. 2021). The mechanical strength of structural lumber is rapidly and precisely detected, evaluated, and classified into different grades based on the flexor elastic modulus and defect distribution characteristics (particularly the knot distribution), in accordance with the load-bearing requirements of wood constructional buildings (Zhao et al 2019). The various stress structures of large-span and multi-high-rise buildings are applied with graded lumber. It is a key factor in enhancing the overall rate of building material use as well as the safety quality of wood construction (Gu et al. 2010, Qiu et al. 2019, Blokland et al. 2021).

A common structural timber species, Fujian Chinese fir (*Cunninghamia lanceolata* (Lamb.) Hook; FCF) has a broad planting area and mechanical and physical attributes like strong impact, straight texture, fine structure, and resistance to corrosion (Tian et al. 2021). FCF lumber is distinctive when compared to other wood species, and many of the existing algorithms are challenging to use to identify FCF defects (Su et al. 2021). Because more dead or live branches

The authors are, respectively, Doctor, Professor, Doctor, Doctor, Doctor, Doctor, Research Institute of Wood Industry, Chinese Academy of Forestry, Beijing 100091, China (mji@caf.ac.cn, wzhang@caf.ac.cn [corresponding author], gfwang@caf.ac.cn, dxliang@caf.ac.cn, miaohu@caf.ac.cn, gaorui0909@21cn.com). The data sets generated during and/or analyzed during the current study are available from the corresponding author upon request. This article was received for publication in September 2023. Article no. 23-00050.

Forest Prod. J. 74(2):185–202.
doi:10.13073/FPJ-D-23-00050

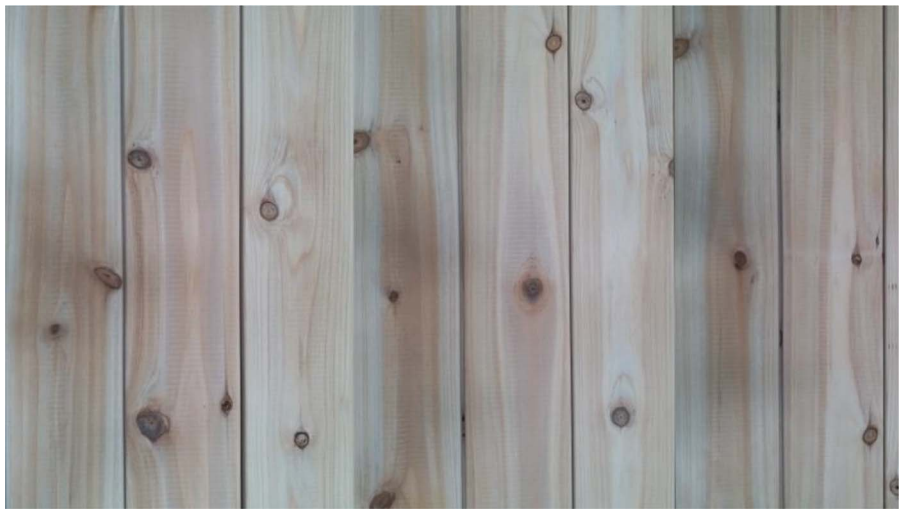

Figure 1.—Fujian Chinese fir constructional lumber.

are buried in the main branches or trunk of FCF during growth, structural lumber displays noticeable knot defects (Kang et al. 2017). Furthermore, additional knots will develop in the FCF tending process as a result of both natural and artificial trimming, which is not optimal (Yue et al. 2020). In contrast to other tree species, FCF lumber has a relatively high ratio of knot diameter to width of the lumber (Wang et al. 2020b). The FCF knot weakens the wood's strength, tilts the wood fiber, and ruins the homogeneity of the lumber structure (Yue et al. 2017). FCF lumber has a higher degree of hardness in dense knot areas, which makes it more difficult to saw, and more prone to cracking when dry. These factors significantly lower the amount and grade of structural lumber available (Zhan et al. 2019). Identifying the knot defect in the FCF lumber is therefore very important for the safety domain stability of the application of wood construction materials (Kopp et al. 2020, Burawska-Kupniewska et al. 2021).

With the advancement of science and technology, the processing and production of wood are moving toward automation, intelligence, and flexibility (Kopp et al. 2020). This calls for the use of sophisticated technical tools to replace manual and traditional methods of defect detection (Yuan et al. 2020). Technological methods employed in the wood processing sector nowadays include ultrasonic, X-ray, stress wave, and machine-vision detection in addition to manual visual inspection (Tu et al. 2021). In recent times, machine-vision detection has gained popularity as a detection technology and is being used in various industries, including manufacturing, construction, and medical (Castellanos et al. 2021). Instead of employing the human brain and eyes, this technology uses computer processors and cameras to analyze the images for target detection. As image processing technology keeps continuing to advance, machine-vision technology affords more options for developing wood inspection business methods.

High automation, high detection accuracy, and high detection efficiency are some of the advantages of machine-vision inspection over other nondestructive testing techniques including stress wave, ultrasonic, X-ray, and others (Kamal et al. 2017). The visual grading and machine grading methods for structural timber were compared by M. Brunetti et al. (2016) of the University of Turin in Italy. The results of the study indicated that the machine grading has an elevated level of flexibility and may significantly boost production efficiency. Two feature detection algorithms were coupled by T. Pahlberg et al. (2015) of Lulea University of Technology in Sweden to look into the automatic matching and recognition procedure for Scottish pine(Pinus sylvestris) lumber. A new machine vision–based approach for the automatic detection of structural lumber was proposed by K. Kamal et al. (2017) of the National University of Science and Technology in Islamabad, Pakistan. The approach uses a feed-forward back-propagation neural network, texture feature extractor, and gray co-occurrence matrix as classifiers. Gray co-occurrence matrix, local binary mode, and statistical moment methodologies have been incorporated by A. Mahram et al. (2012) of Urmia University in Iran to provide superior feature extraction techniques and patterns for knot classification and recognition. The dimension eigenvector has been diminished using principal component analysis, linear discriminant analysis, support vector machine, and K-nearest neighbor.

The most widely utilized techniques currently in use for image identification of large-size structural lumber (the lumber length range in this research is greater than 4,000 mm) are image pyramid, multiscale sliding window detection, data enhancement, and image segmentation recognition (Viguier et al. 2017, Wang et al. 2020a, Pang et al. 2021). Nevertheless, the aforementioned techniques for small-target picture recognition necessitate a more complicated program structure and a more complex target recognition model (Ramage et al. 2017, Panwar et al. 2020, Longo et al. 2019). Even so, there are certain drawbacks with this approach, including low defect detection efficiency and subpar real-time performance in applications that are practical. This is mostly since imperfections constitute only up to a tiny fraction of the large-size image of the lumber's exterior (Ashok et al. 2021, Wright et al. 2019). The "invalid" identification employment consumes an enormous amount of time during the defect detection process for lumber images if the entire surface image is acknowledged by the deep learning algorithm model (Pan et al. 2021). Prior to the method's determination, we investigated the detection technique. In conjunction with the

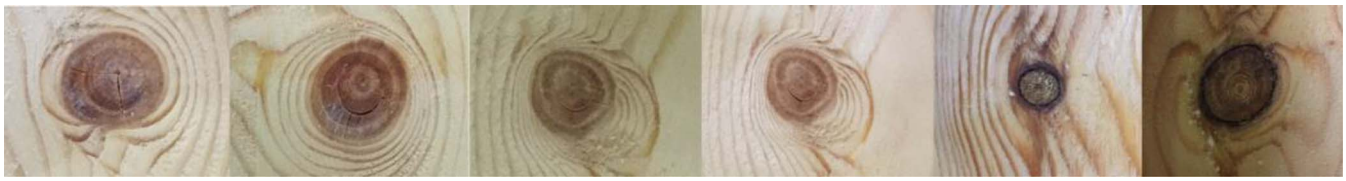

Figure 2.—Characteristics of knots of Fujian Chinese fir constructional lumber.

features of large-size FCF sawn timber detection, the YoLo algorithm's sizing is limited to 640 pixels by 640 pixels for input images; for sawn timber sizes greater than 2 m (2,048 pixels by 24,576 pixels), the algorithm is ill-suited for large-scale sawn timber detection. Thus, we developed a technique to identify FCF knots.

This work presents an approach of locating, detecting, and conducting digital nondestructive testing of enormous lumber knot defects via image defect features in order to address the issues with the tiny-target detection process of large-sized lumber. Locating and searching for FCF defects is an essential initial stage toward assessing the mechanical qualities of FCF plantation structural wood. Then, we sawed structural lumber according to the characteristics of FCF and the large-size lumber knot detection and positioning result, and carried out mechanical tests to explore the effect of different knot positions on the mechanical tests of sawn timber, in order to further improve and optimize the machine-vision knot detection system. We have developed our own equipment for testing and grading the mechanical properties of structural sawn timber, and we hope to establish a link between mechanical stress grading and machine-vision grading, and further combine the advantages and shortcomings of the two testing methods. This procedure will also yield essential preliminary data for the structural design and performance enhancement of structural lumber bearing materials, hastening the use of structural wood in China's industrial sector.

Materials and Methods

Materials

For the experiment, FCF of the second generation from Shunchang County, China, was utilized. The collection of FCF complied with relevant institutional, national, and international guidelines and legislation.

The trees were between 20 and 30 years old, with a 180- to 250-mm diameter at breast height. The moisture content of the tested FCF constructional lumber (CL) is between 12 and 15 percent, in accordance with EN 13183-1:2002 (The European Standard EN 13183-1:2002). FCF CL has an average density of 0.40 g/cm^3. A number of timber pieces featuring varying surface knots were chosen in order to assess and confirm the viability of the search and localization strategy used in this investigation. The Shengsheng Wood Industry Co., Ltd., in Shunchang County, Fujian Province, China, completed the factory application experiment (Figs. 1 and 2; Table1).

Table 1.—The density of Fujian Chinese fir.

Tree species	Density	Average
Fujian Chinese fir	0.3–0.5 g/cm^3	0.40 g/cm^3

Methods

By combining the surface characteristics of the FCF CL, we created a reliable knot localization algorithm. To locate knots in FCF CL, a scanning image was processed using the proposed approach. After the logs were cut into 40 by 140 by 4,000-mm lumber, it was further processed into several 17 by 38 by 330-mm little test specimens. The machine-vision technology was utilized to scan the image of the lumber using the four-faced sawing method. An algorithm was then used to process the acquired image in order to locate and search for knots in the FCF CL. The primary hardware components needed for the machine-vision system we designed are a camera, a light source, an encoder sensor, photoelectric sensor. The image that was gathered has 24-bit RGB color, resolution 204812288, and 300-lx illumination. Ultimately, using mechanical testing machinery, the impact of knots on the bending resistance of FCF CL was investigated. Figure 3 depicts the research procedure for finding knots of the FCF CL. The height is represented by a thickness of 17 mm. When sketching, we visually exhibit the width side in the graph to make the knot evident to the reader. Five hundred pieces of lumber were put to use in the machine-vision knot-localization detection experiment. We performed six groups of mechanical testing on FCF CL during the three-point mechanical experiment, with 20 specimens in each group. The average density of FCF CL in two sets of studies was 0.3 to 0.5 g/cm^3, and the FCF CL had knots that were dispersed randomly across the surface of timber samples.

Compared to the visual grading method, machine-vision grading is a more efficient and practical grading approach. Knots primarily affect a lumber's mechanical qualities. The knot area and nonknot area of structural lumber's gray values were processed using the FCF knot anisotropy and gray characteristics. A number of vacuum areas far from the knots were deleted, the misfitting issues other than the lumber knots were resolved, and the loss of edge information was successfully prevented. It was discovered that the edge of the FCF knots encircled the protruding and connected area. Small holes were filled, the fractures in the contour line were divided, the narrow discontinuities and thin gullies that arise in the knot placement were bridged, and several small-connected knots were divided. In order to improve position identification accuracy and lessen the impact of the FCF's surface properties on knot feature extraction, we merged the aforementioned techniques. A wave trough, or groove, occurred at the profile line in the gradient change of the gray-value contour line. The knot region was searched, the knot's contour was fitted, and the knot's position was further investigated. Figure 4 depicts the search for knots of the FCF CL. We have been attempting to investigate and establish a connection between the mechanical characteristics of sawn lumber and visually observed knot problems. The

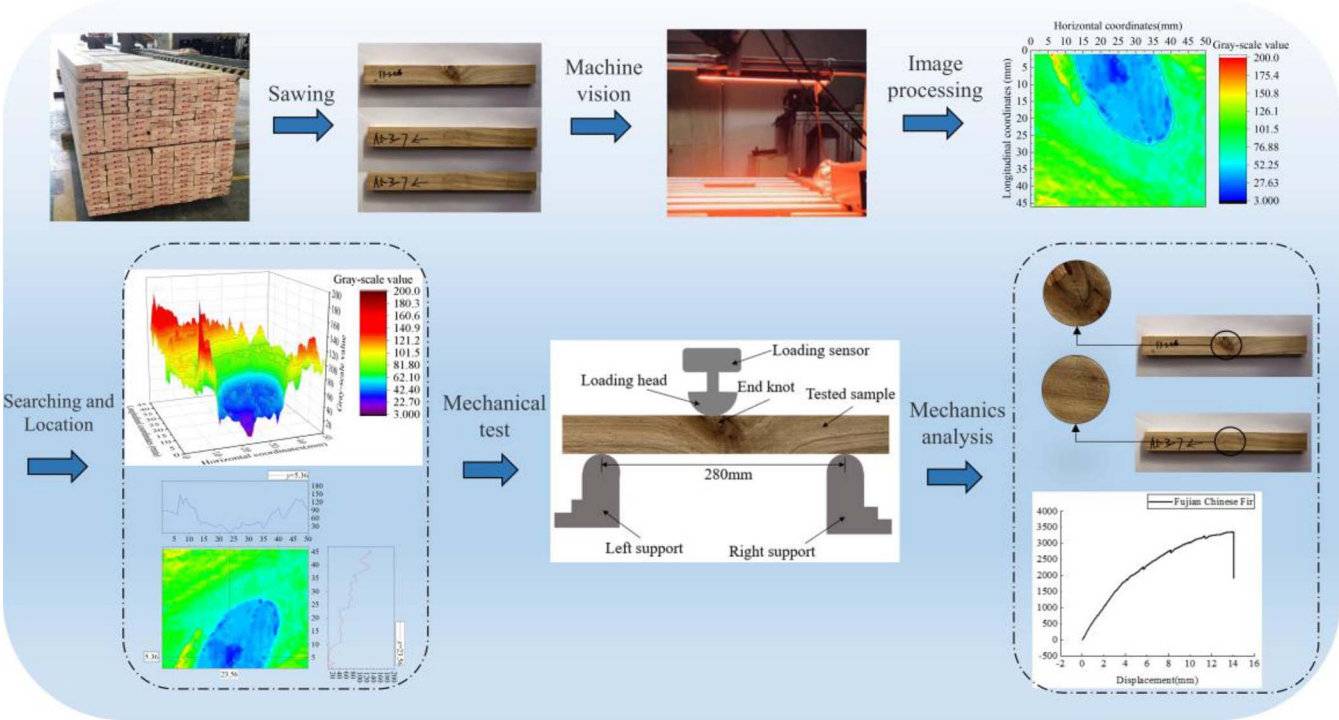

Figure 3.—The procedure for locating knots in Fujian Chinese fir constructional lumber.

"Results" section "Effect of knots on bending resistance of FCF CL" examines the impact of knots in various locations on the mechanical characteristics of mechanically sawn timber, as knots play a significant role in lowering the mechanical properties of sawn lumber. It is intended that the sawn timber would be evaluated through statistical consideration and analysis of knots and knot position.

We divided the knots of FCF sawn timber into dead knots and live knots, and the live knots were further divided into round knots and edge knots, as shown in Table 2. The positioning method introduced is able to discern three kinds of knot color changes.

Structural design of lumber detection system based on machine-vision technology.—The sensors of the image data acquisition and detection equipment mainly capture images from the camera and red-stripe light source. The horizontal measuring instrument is used to measure the angle between the light source and the camera in a vertical direction. The FLUKE illuminometer is used to measure the illumination of the light source. The position of the detection system sensor and light source is shown in Figure 5. We adjusted the inclination degree of the strip light and the vertical angle between the camera to 60° and kept it fixed. A light source device was designed which can automatically adjust the height and brightness. The device had a wide transverse radiation range and high brightness to better distinguish the object from the background. By adjusting the appropriate light source, the characteristics of FCF could be clearly captured, which was conducive to the processing and analysis of the acquired images.

We scanned and imaged the bark stump face image data of the tree species. The camera scanned the image data under the lens and sent the final image to the computer for image processing. Different tree species were photographed using a Basler raL2048-48 gm line-scan camera with 2,048 pixel per line resolution and 51 kHz line-scan rate. The camera was from the German Basler manufacturing company, located in Ahrensburg, Germany, founded in 1988, which, with 30 years of experience in the field of vision technology, is the world's leading computer vision expert. The following

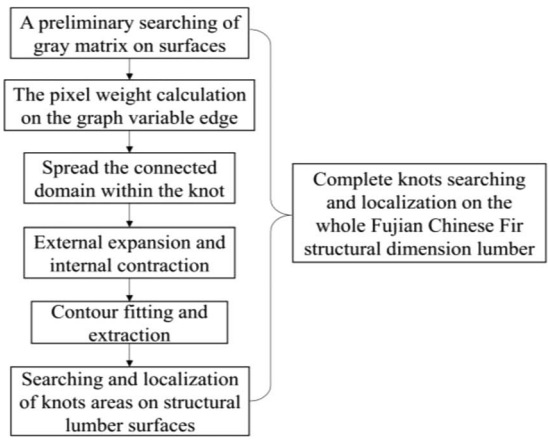

Figure 4.—The algorithm used to locate knots.

Table 2.—Samples image of different types knot defects in Chinese fir sawn timber.

Dead knot		Round knot	
Edge knot		Without defects	

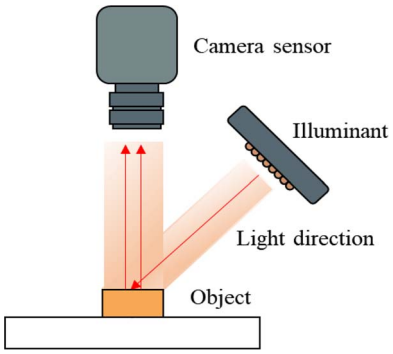

Figure 5.—Image acquisition system.

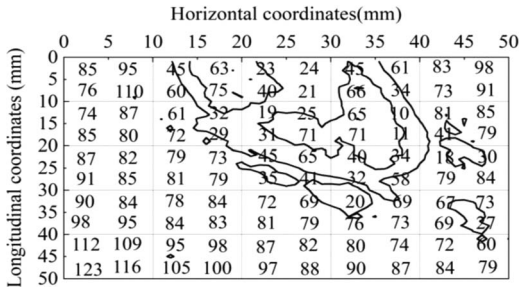

Figure 7.—A knot preliminary searching and location of gray matrix on surfaces of lumber.

is the basic information of the obtained images: 2,048 by 2048 pixels, and a bit depth of 8. First, different tree species images were collected and annotated, then image transformation expansion was performed and finally the tree species' instance segmentation model was trained to achieve tree species recording and recognition.

A preliminary searching of gray matrix on surfaces.—The term "anisotropy" describes sawn timber's varying mechanical and physical characteristics along its grain. Wood's structure causes it to exhibit different strength, elasticity, and other properties along the annual rings (known as the chordal direction), perpendicular to the rings (known as the radial direction), and in the direction of the wood grain (known as the longitudinal or axial direction). Wood is primarily composed of cellulose, hemicellulose, and lignin. For instance, wood often has a substantially higher tensile strength in the direction of the grain than in the chord direction. For wood processing, design, and engineering applications, this anisotropic feature is crucial. It must be used and developed suitably in accordance with the various directional qualities of wood.

Knots are the primary defect in sawn timber, based on the features of the actual FCF. The color of sound knots is a distinct shade of grey relative to parts of wood free of defects. In the manuscript, we display images of both living and dead knots in Figure 6.

In Figure 7, the distribution coordinates have been established, the length direction is the x axis, the width direction is the y axis, and the upper left corner of the lumber is the coordinate origin in the knot search and position of FCF CL.

Each pixel in the grayscale image of lumber was read out, and after median filtering, the proportion of transverse and longitudinal scanning was used to convert the grayscale value into the actual position point coordinates of the lumber (Viguier et al 2015, Kandler et al 2016, Jenkel et al 2018). There were outliers 71 and 75 in the lumber gray value reading, which could be related to the light-colored area that occurs inside the knot. The gray value in the closed-loop connected domain of 60 value also exhibited a dramatic fall. There were outliers of 18, 20, 27, and 35 outside the 60-value closed-loop linked domain. As seen in Figure 7, the sources of the outliers in this region could include digital noise in the images, scanning distortion, light effects, dark stains on the lumber's surface, etc. Outside of the knots, there can potentially be interference regions with the same gray value as the knot. To actualize the high-precision position of FCF CL knots, it is important to cope with the aforesaid interference, eliminate outliers, and connect the small outlier areas inside the knot. Consequently, one of the fundamental and crucial procedures in the processing steps is to read out the gray value of the entire lumber.

The pixel weight calculation on the graph variable edge.—The Gaussian filter function based on spatial distribution ensures the preservation of pixel values near the edge, and excludes pixels far away from the edge without affecting the pixel values on the edge (Lukacevic et al. 2019). By using the spatial filter and distance filter in conjunction with nonlinear fitting to sharpen the image while preserving the characteristics of the knots on the timber surface, the cavity problem in the grayscale image was resolved.

We identified any erratic and unpredictable changes in brightness or color that may be present in the image as graphical noise. The sawn timber knots exhibit nonuniform grey tones and, in certain instances, also exhibit uneven fluctuations in brightness or color. The two aforementioned factors may result in a cavity, which we refer to as a cavity

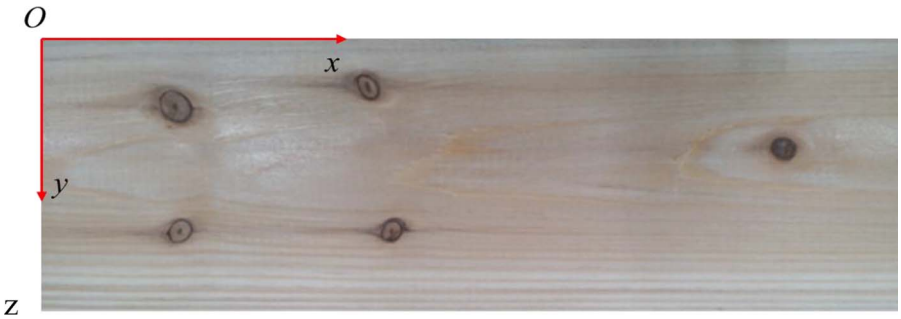

Figure 6.—Coordinates for the distribution of lumber.

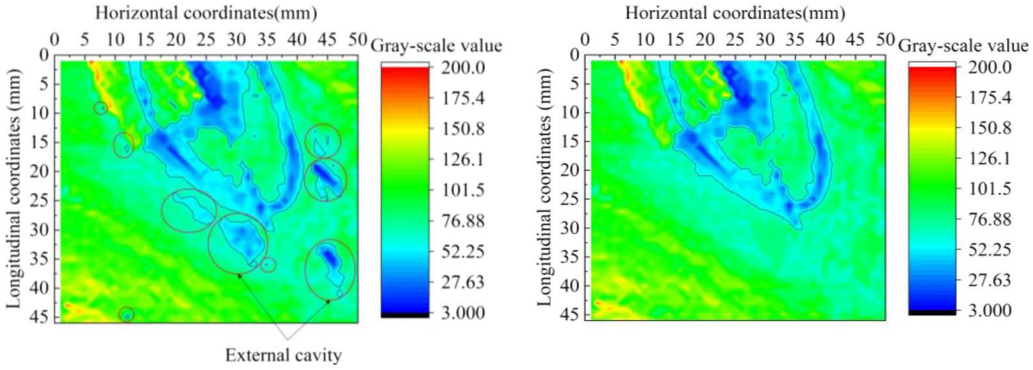

Figure 8.—The pixel weight calculation on the graph variable edge (a) knot searching of Fujian Chinese fir constructional lumber before external cavity removal (b) localization after external cavity removal.

problem, where the middle pixel point of the knots is lower than the surrounding pixel points.

$$\mathrm{BF}(I)_p = \frac{1}{\mathrm{W}_p}\sum_{q\in S}\mathrm{G}_{\sigma_\mathrm{S}}(\|p-q\|)\mathrm{G}_{\sigma_\mathrm{r}}(|I_p-I_q|)I_q \tag{1}$$

where BF(I) describes the bilateral filters, I is the input image, I_p and I_q respectively denote the image value at pixel positions p and q, S represents the spatial domain, and G_σ describes the two-dimensional Gaussian kernel (Tang et al 2018).

The normalization constant $\mathrm{W_p}$ is defined as follows:

$$\mathrm{W}_p = w(i,j,k,l) = w_\mathrm{s}(i,j,k,l)\times w_\mathrm{r}(i,j,k,l) \tag{2}$$

$$\mathrm{W}_p = \sum_{q\in S}\frac{1}{4\pi^2\sigma_\mathrm{s}^2\sigma_\mathrm{r}^2}\exp\left(-\frac{(i-k)^2+(j-l)^2}{2\sigma_\mathrm{s}^2}-\frac{\|f(i,j)-f(k,l)\|^2}{2\sigma_\mathrm{r}^2}\right) \tag{3}$$

where $w(i,j,k,l)$ describes spatial domain kernel template weight, $w_\mathrm{s}(i,j,k,l)$ describes value domain kernel template weight, $w_\mathrm{r}(i,j,k,l)$ describes bilateral filter template weight, (i,j) describes the position of the relevant pixel around the target pixel, $f(i,j)$ represents pixel value, (k,l) represents the position of the target pixel, $f(k,l)$ represents the pixel value of the target pixel, σ_s is distance standard deviation of Gaussian function, and σ_r is the gray standard deviation of Gaussian function (Yang et al 2018, Gao et al 2019).

The objective of the algorithm's detection is to remove several cavity areas that are far from the knots in order to identify mismatches that happen outside of the lumber knots and prevent the loss of edge information (Fig. 8a). The spatial domain weight is significant in the region where the lumber image's gray value is flat, the point where pixel change is minor, and the corresponding pixel range is close to 1. Currently, it is possible to process certain unnecessary gray change values outside of the knot to prevent areas without knots from being mistakenly identified. In the edge area of the knots, the difference in gray between the pixels is large, the pixel range domain weight is large, the spatial domain weight is small, and the edge information can be obtained. The processing effect diagram is shown in Figure 8b.

Spread the connected domain within the knot.—By analyzing a knot's pixel value, we were able to determine that certain localizations in the interior region of the knot had higher pixel values than others. These points can be attributed to the inherent qualities of wood. The situation mentioned above will affect the precise detection of the knots on the surface of FCF. Based on the area-filling principle, the connected domain with the internal interference areas within the knots is treated by using the spreading domain method.

Based on the area-filling method, starting from one pixel P (x, y), P (x, y) spreads in eight surrounding vector directions (Table 2) to achieve the denoising effect (Yu et al. 2020). The spreading logic is this: if there is no filling, fill it (Singh et al. 2020); if it is filled, continue to search for the neighboring pixels in each of the eight vector directions with these eight pixels (Fig. 9) until the enclosed area is completely spread or spread to the predetermined boundary

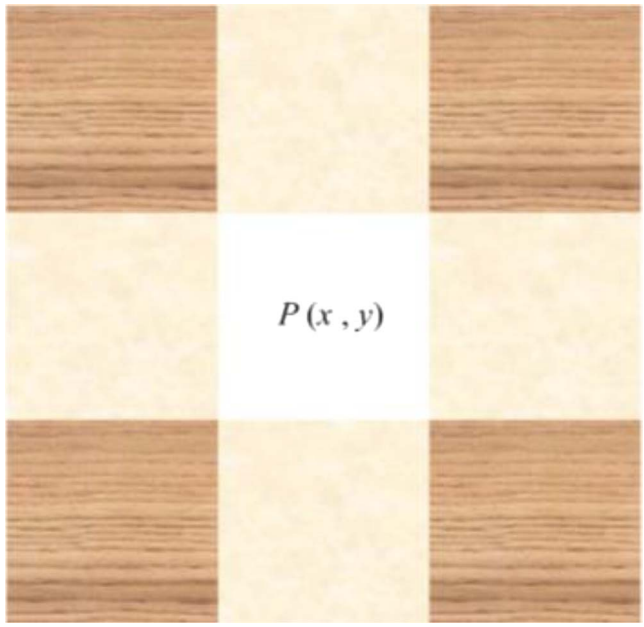

Figure 9.—Eight-neighborhood point search.

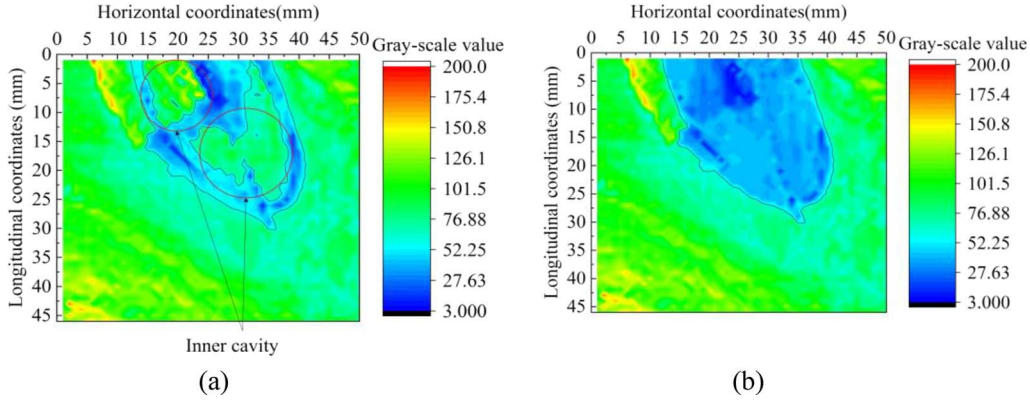

Figure 10.—Spread the connected domain within the knot (a) knot localization of Fujian Chinese fir constructional lumber before inner cavity removal (b) knot localization after inner cavity removal.

of the knot. This operation provides important help for contour extraction and region separation.

The calculation method of the boundary point vector is as follows:

The color and texture characteristics of FCF CL are not uniform. In the detection process, there are often some adjacent closed areas in a knot, which will affect the localization and detection of the knot (Fig. 10a). Applying eight-neighbor spreading the connected domain method to fill adjacent pixels, which can spread from a closed area in a knot to other areas, mark or separate a part of the image of a lumber for processing and analysis. Check whether the current pixel has the original color of the region (Li et al. 2021, Shuaeb et al. 2021). If the answer is yes, fill the pixel in the recursive call, and use each adjacent pixel as a new seed; if the answer is no, the current pixel is returned to the caller. In this paper, the spreading the connected domain algorithm is used to extract the central part of the knot, starting from a point (initial point), and traversing nearby pixels. Using this method, the protruding area surrounded by the edge of the knots can be found in the pith of lumber, and the interconnected area surrounded by the knots can be found initially (Fig. 10b). The algorithm successfully solves the problem of individual knots being separated or narrowed, and the calculation is simple and fast.

External expansion and internal contraction.—Through the external expansion and internal contraction operations, the basic features of the lumber can be further extracted, and then a higher-level algorithm can be used to identify the knots. The algorithm filter is defined by a planar or nonplanar structural element, which is usually moved by pixel on the image and is comparatively processed in the corresponding mask. The knot of lumber is expanded externally and then contracted internally. The image of knots maintains the original shape and changes the geometry evenly. In the process of internal contraction, the specified edge point of the internal contraction direction is used as the contraction point (Damme et al. 2021).

Use vector addition to merge two sets, such as (a,b) + (c,d) = (a + c, b + d). External expansion X⊕B is the set of all vector sums. The two operands of vector addition come from X and B respectively, and obtain any possible combination (Zhang et al. 2020). Let X and B be the set of two-dimensional integer space P, X is defined by B extension as:

$$X \oplus B = \left\{ p \in \varepsilon^2, p = x + b, x \in X, b \in B \right\} \tag{4}$$

X is expanded by B is the set of all expanded areas, where B is often called a relative structural element, and the input image is translated by all points of the structural element, and then the union is calculated to obtain the result. The filled area is the result of external expansion, and the filled area includes all the ranges of X. This operation can merge the points around the image into the object, or connect two similar areas in a knot area. Therefore, it is very useful to fill in the cavities in the image, and at the same time, the operation has a filtering effect on the outside of the image of knots (Ma et al. 2020, Valle et al. 2020).

X is defined by B internal contraction as:

$$X \Theta B = \left\{ p \in \varepsilon^2, p + b \in X, \forall b \in B \right\} \tag{5}$$

Internal contraction of X using B is a set translation of all points in B that are contained in X. The filling area is the result of indentation, and the filling area contains all ranges of X. This operation is a contraction process to shrink the target set, so it can eliminate useless points or small area components in the image, and it can also separate two small connected knots, which has a filtering effect on the image.

Let $\overset{\cup}{B}$ be the symmetrical set of B about the reference point, which also becomes the transpose. According to the Equation 6, the expansion operation can be used to realize the contraction operation.

$$(X \Theta B)^C = X^C \oplus \overset{\cup}{B} \tag{6}$$

Expanded in eight directions, the image of knots can maintain the original shape. However, when expanding in a single direction, some expansion points are not within the range of the vector table, so there will be a problem that the points that should be expanded cannot be expanded.

There are several ways to solve this problem (the eight directions of the boundary vector are shown in Table 2).

(1) When the vector from this point to the next boundary point is 1, and the expansion direction is 3, if the upper adjacent point (90° direction) or the right adjacent point (0° direction) of

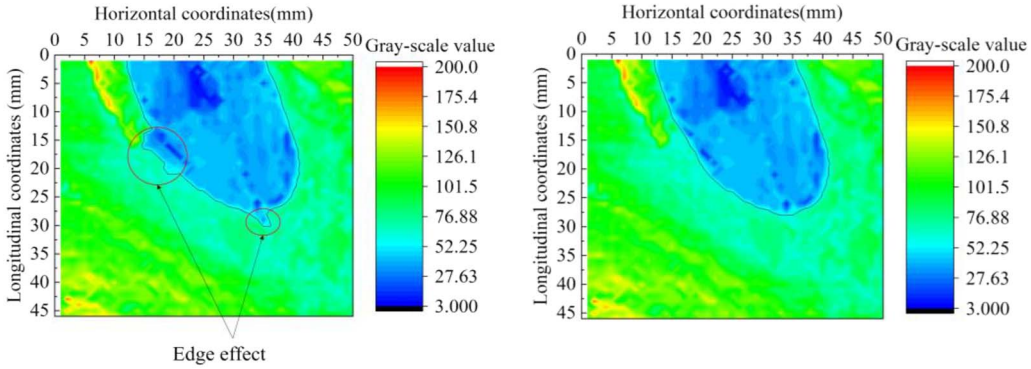

Figure 11.—Spread of the connected domain within the knot. (a) Knots localization of lumber before inner cavity removal. (b) Knot localization after inner cavity removal.

this point is "1," extend the points with 1. (2) When the vector from this point to the next boundary point is 3, and the expansion direction is l, and when the lower adjacent point of the left adjacent point of this point is 1, then 1 or the left adjacent point of this point should be expanded. (3) When the vector from this point to the next boundary point is 5 and the expansion direction is 1, if the adjacent point or lower adjacent point of this point is 1, the left or lower adjacent point of 1 is expanded. (4) When the vector from this point to the two boundary points is 7, and the expansion direction is 1, if the adjacent point or lower adjacent point of this point is 1, the right or lower adjacent point of 1 should be expanded. In the process of internal contraction, the key question is how to choose edge points. If there are more than two boundary points on a straight line, and the vector and the internal contraction direction are the same, only the two end points on the straight line can be contracted on the edge points in the internal contraction direction.

In the process of the contours fitting of knots of CL, if there is a strong light and dark change in the image of knot, that is, there are large changes in the adjacent contours, the knot contours of the point can be extracted. When this algorithm is not applied, the edge error recognition effect is obvious (Fig. 11a). By selecting appropriate structural elements to carry out outward expansion and inward contraction operations on knots of lumber, it can bridge the narrow discontinuities and slender gullies in knot positioning, eliminate small cavities, fill the fracture of contour line, and separate two (or more) small connected knots (Fig. 11b).

Measurement of knot areas on structural lumber surfaces.—On the surface of FCF lumber, the gray matrix of the knot area and the nonknot area has a large difference, the knot has obvious edges, and there are usually multiple gradients on the edge of the knot. If the gradient value appearing at a certain point is large, it means that the light and dark changes of the image at that point are relatively large, and the morphological edge detection would consider that there is an edge.

The effect picture after use by a canny operator for edge detection can be seen in Figure 12: the processed picture removes the background and foreground from the image, leaving only the edge contour of the background and foreground; the method is able to extract the outer contour of the whole sawn timber as well as the edge of the knot in a clear and complete manner, and is able to meet the expected requirements of the test. The system is able to identify and completely label the sawn timber with a rectangular box to completely differentiate it from the background, and at the same time use an ellipse plus a rectangular box to mark the identified surface defects of the sawn timber.

In this study, machine-vision and image processing methods were used to eliminate the influence of anisotropy of lumber and knot on the knot size measurement, and to compare the surface defect contour changes of lumber. The optical effect is used to scan the gray value changes of the image of lumber to estimate the knot area and fit the knot contour. Finally, the minimum enclosure rectangle fitting the algorithm is used to determine the size of the knot.

Any point was set on the edge-fitting closed curve C as $P(x_i, y_i)$, and the minimum and maximum horizontal and longitudinal coordinate values on the closed curve were calculated to be x_{min}, x_{max}, y_{min}, and y_{max}, as shown in Equations 7 through Equations 10:

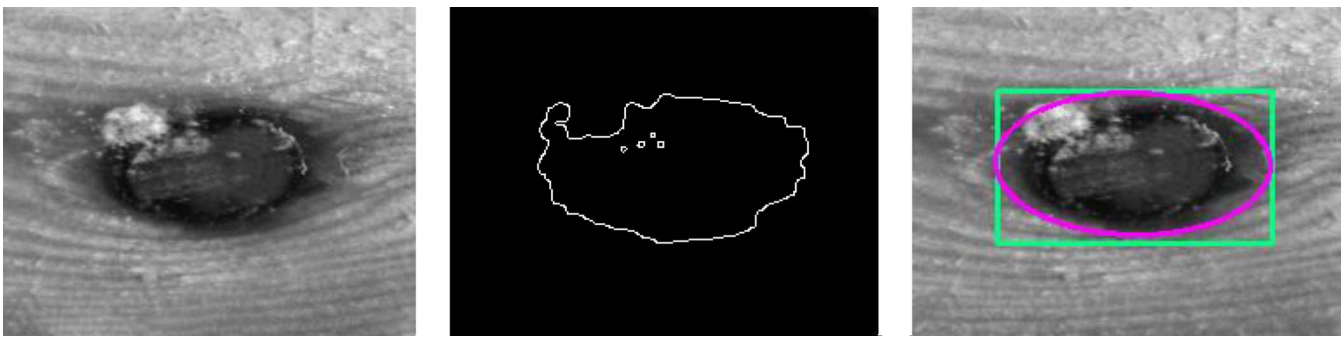

Figure 12.—Knot edge detection and fractal technique.

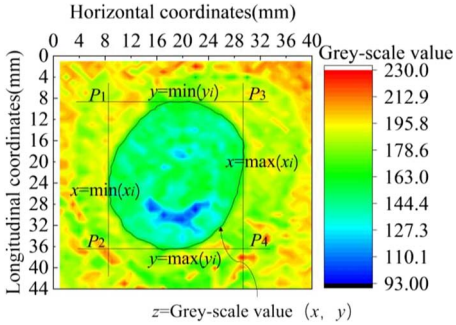

Figure 13.—Calculation of the knot size based on the minimum enclosure rectangle method.

$$x_{\min} = \min(x_i) \tag{7}$$

$$x_{\max} = \max(x_i) \tag{8}$$

$$y_{\min} = \min(y_i) \tag{9}$$

$$y_{\max} = \max(y_i) \tag{10}$$

The four-point coordinates $P_1(x_{min}, y_{min})$, $P_2(x_{min}, y_{max})$, $P_3(x_{max}, y_{min})$, $P_4(x_{max}, y_{max})$ of the minimum enclosure rectangle of the closed contour were calculated. Finally, the length (L) and width (W) of the knot were calculated, as shown in Figure 13.

$$L = |x_{\max} - x_{\min}| \tag{11}$$

$$W = |y_{\max} - y_{\min}| \tag{12}$$

In the gradient change of the gray value contour line, if there is a trough (groove; Fig. 10b), the knot near the area was searched as shown in Figure 10c. The contour-fitting extraction algorithm connected the points with the same gray matrix value of the lumber to form a ring line and directly project to the plane to form a horizontal ascent contour line (Fig.10d), and the ring lines of different heights would not coincide, which achieved the purpose of extracting the contour of the knot. According to the type and characteristics (color, lighting, etc.) of lumber, the knot gray value contour algorithm was used to draw the contour-fitting graph, so as to measure different types of size (Fig. 14).

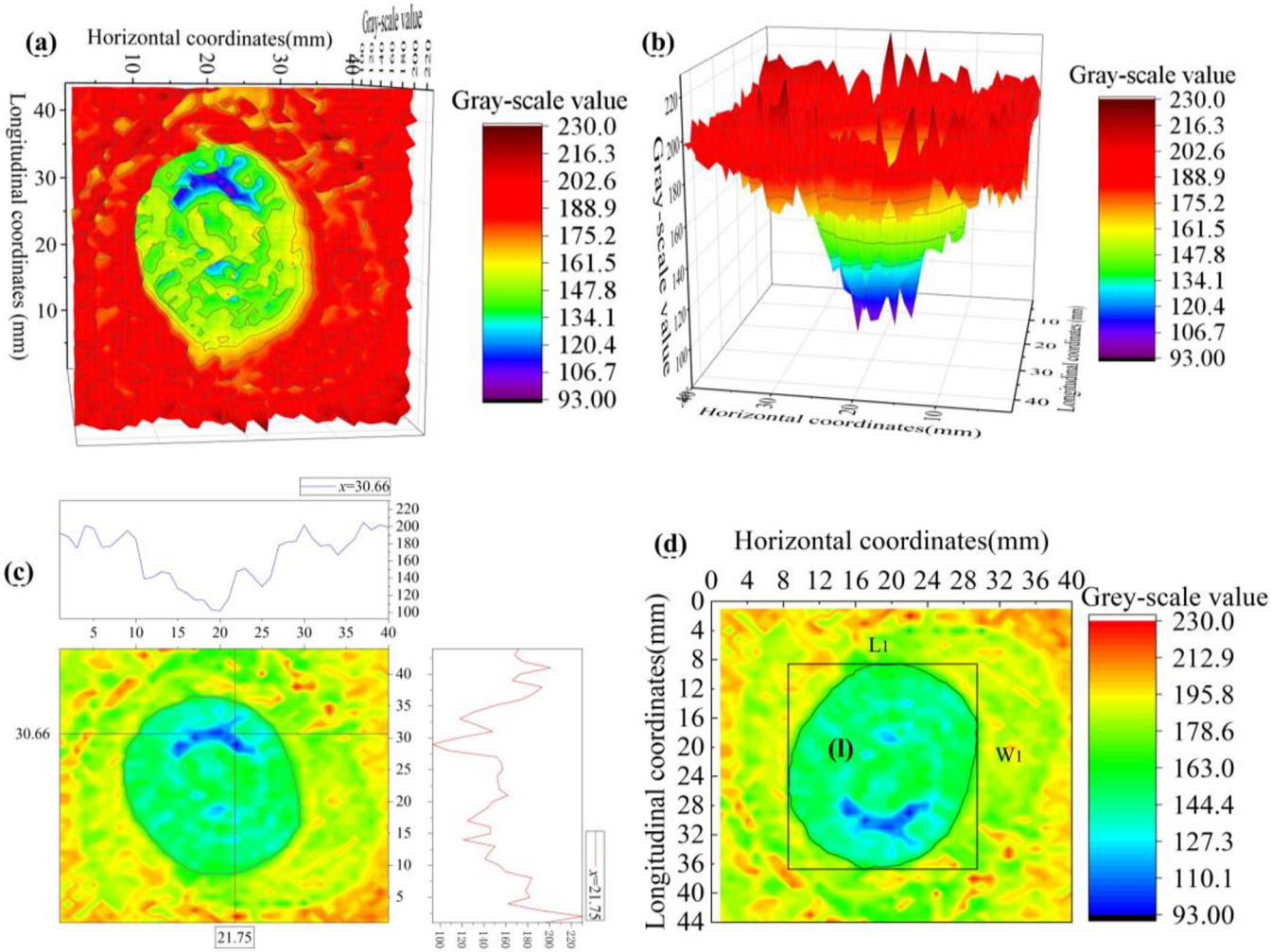

Figure 14.—Size measurement of knot areas on the surfaces of Fujian Chinese fir constructional lumber: (a) contour three-dimensional (3D) mapping curve, (b) projection of 3D mapping curve, (c) contour sectional graph, and (d) edge contour fitting and oval knot size graph.

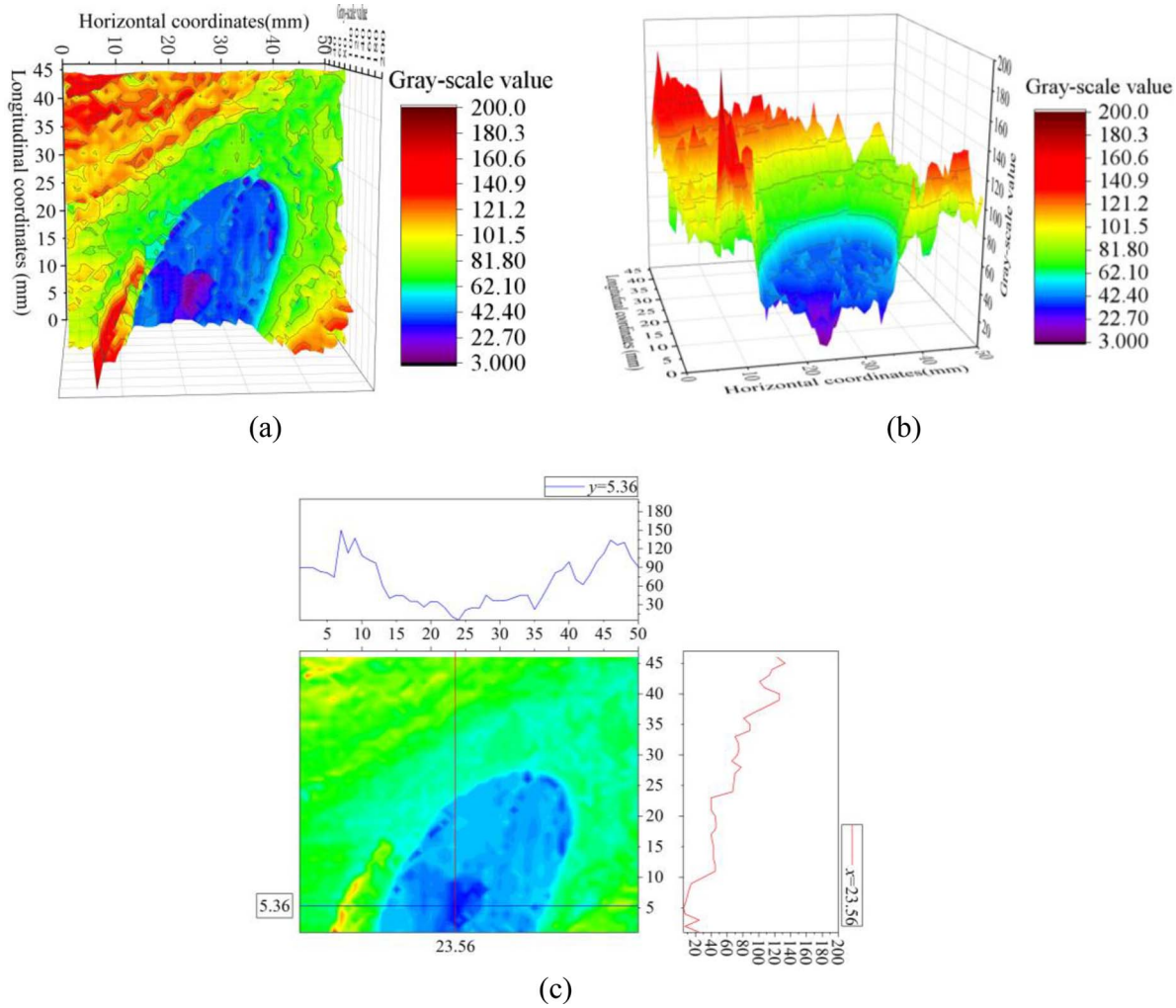

Figure 15.—Research and localization of knots area on structural lumber surfaces: (a) projection of three-dimensional (3D) mapping curve, (b) contour 3D mapping curve, and (c) contour sectional graph of knot.

Searching and localization knots areas on FCF CL surfaces.—There is a binary function z = f(x) for the gray scale of lumber, which considers the rate of change of the function in any direction at a certain point. Consider ray l emitted from the point P(x, y). The ray refers to a directional half-line. Take a point P′(x + Δx, y + Δy) near the point P(x, y) in the l direction, denoted as |PP'| = ρ. That is $\rho = \sqrt{(\Delta x)^2 + (\Delta y)^2}$. The directional derivative of the function point P along the direction l (the limit value exists) is:

$$\frac{\partial f}{\partial l} = \lim_{\rho \to 0} \frac{f(x + \Delta x, y + \Delta y) - (x, y)}{\rho} \tag{13}$$

The directional derivative is the rate of change of the function z along the half-line.

In the FCF CL, the gray matrix of the knot area and the nonknot area has a large change, the knot has obvious edges, and there are usually multiple gradients on the edge of the knot. If the gradient value appearing at a certain point is large, it means that the light and dark changes of the image at that point are relatively large, and the morphological edge detection will consider that there is an edge.

The known directional derivative formula follows:

$$\frac{\partial f}{\partial l} = \frac{\partial f}{\partial x}\cos\alpha + \frac{\partial f}{\partial y}\cos\beta = \vec{G} \cdot \vec{1}^{0} = |\vec{G}|\cos(\vec{G}, \vec{1}^{0}) \tag{14}$$

When $\vec{1}^{0}$ and $\vec{G}$ have the same direction, the direction derivative takes the maximum value max(∂f/∂) = $|\vec{G}|$.

This study is realized by comparing the changes in the contours of the surface defects of the lumber. Combined with the characteristics of FCF, the gray value change of image of lumber is scanned, and the knot edge contour is fitted and extracted to position knot area of lumber. The pith of the lumber knots of FCF CL is often darker, and the color depth is gradually reduced in the form of the pith gradually radiating outward, showing a trend of gradient change of the gray value contour. The contour-fitting extraction algorithm connects the points with the same gray matrix value of the FCF CL to form a ring line and directly project to the plane to form a horizontal ascent contour line (Fig. 15a), and the ring lines of different heights will not coincide. In the gradient change of the gray value contour line, if there is a trough (groove; Fig. 15b), search and locate the knot near the area, as shown in Figure 15.

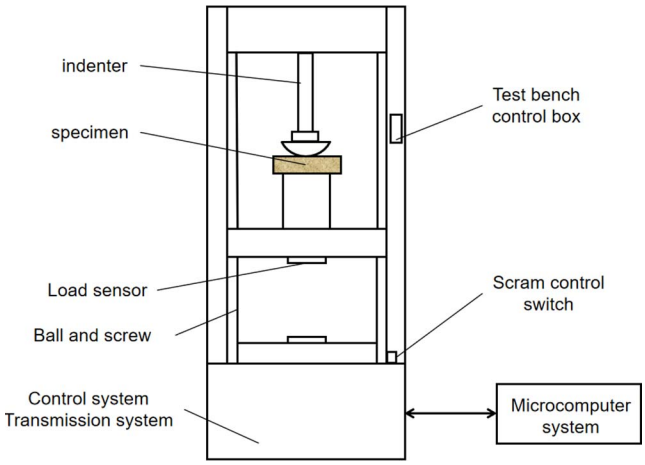

Figure 16.—Sawn timber mechanics testing machine structure diagram.

Based on the introduction in the previous "Methods" sections, the knot searching and localization steps for lumber are as follows: through the lumber and background segmentation, determine the coordinate origin of the overall surface of the lumber, and establish the coordinate system of the surface of lumber. The characteristic information of the image is preserved in the spatial domain. With recursive search as the core, the designated color in the Unicom area is replaced from the designated position to eliminate the small outlier area. The target point is merged into the lumber background and expanded to the outside, and the regions with large differences in gray value inside the target knot can be merged, which is convenient for extracting the whole knot. Eliminate the connected boundary of adjacent nodes, contract the boundary inward, separate the knots of different objects that are stuck together, and remove small particle noise. According to the type and characteristics (color, lighting, etc.) of FCF CL, use the knot gray value contour algorithm to draw the contour fitting graph, so as to search and locate the knot (Fig. 15c).

FCF three-point bending test.—The specimen is subjected to a three-points bending test with a Instron 3369 microcomputer electronic universal mechanical testing machine. The test loading procedures refer to the GB/T 50329-2012 standard for test methods of timber structures and GB/T 1936.1-2009 test methods for bending strength of timber. The tested specimens span-to-depth ratio is (17:280) = 16.5, the thickness of the specimens is 17 mm, and 38mm is the loading surface of the indenter. According to the standard GB/T 1936.1-2009, the effect of component of shear deflection is ignored. The main contents measured in the test include midspan deflection value and breaking load of the specimen. The whole loading process is controlled by displacement, and the three-point bending test is carried out at a constant loading speed of 5 mm/min, and applying pressure on the narrow side and continuing loading until the specimen is damaged. The duration is 2 to 3 minutes.

According to the standard GB/T 1936.2-2009, method for determination of the modulus of elasticity in static bending of wood, multiple applications and load releases are made to stabilize the deflection measurement to obtain true deflection. Generally, we do not consider the deflection of the initial compressive test. After adjusting the test several times according to the steps introduced in the standard, the real value of specimen deformation between the upper and lower loads is obtained from the subsequent test results for modulus of elasticity (MOE) calculation.

In the three-point bending test, during the vertical compression of the load head in the specimen, the lower and upper limit load for measuring the specimen deformation is generally 300 to 700 N. The testing machine first loads the lower limit load at a uniform speed, and immediately records the dial indicator value, accurate to 0.005 mm. Data is recorded in the table, and then the machine loads to the upper limit load after 15 to 20 seconds, then unloads; this is repeated three times, and each time the unloading should be slightly lower than the lower limit load, and then the load lowers to the lower limit load, and finally the deflection change is determined as the true value of the sample deformation between the upper and lower limit loads. We do not consider the initial deflection, and finally obtain the real deformation value of the sample between the upper and lower loads after the above test for MOE calculation.

According to GB/T 26899-2011 for structural laminates and GB/T 50708-2012 for structural design specifications for glulam wood, the laminates are composed of preforms. Pubon glue is used as the adhesive. The moisture content of the laminates is between 8 and 15 percent, and the pressure applied during the lamination is controlled between 0.6 and 1.0 MPa. The three-point bending test was carried out by using a YAW-1000Fweiji control electro-hydraulic servo wood bending strength testing machine, which combines electronic technology with mechanical transmission technology. The deflection and load signals were collected in real time and displayed synchronously through the digital display window on the software.

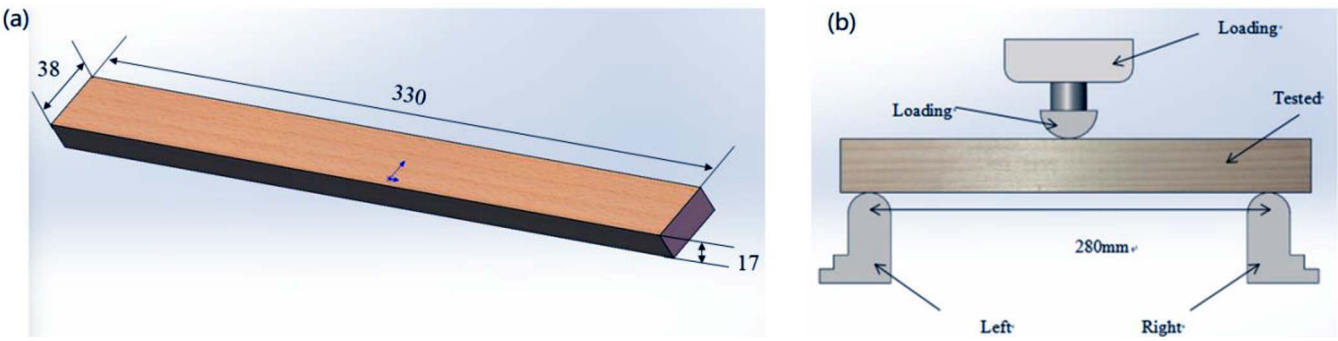

Figure 17.—Three-point bending test: (a) dimensions of the specimen, and (b) model of three-point bending test.

(a)

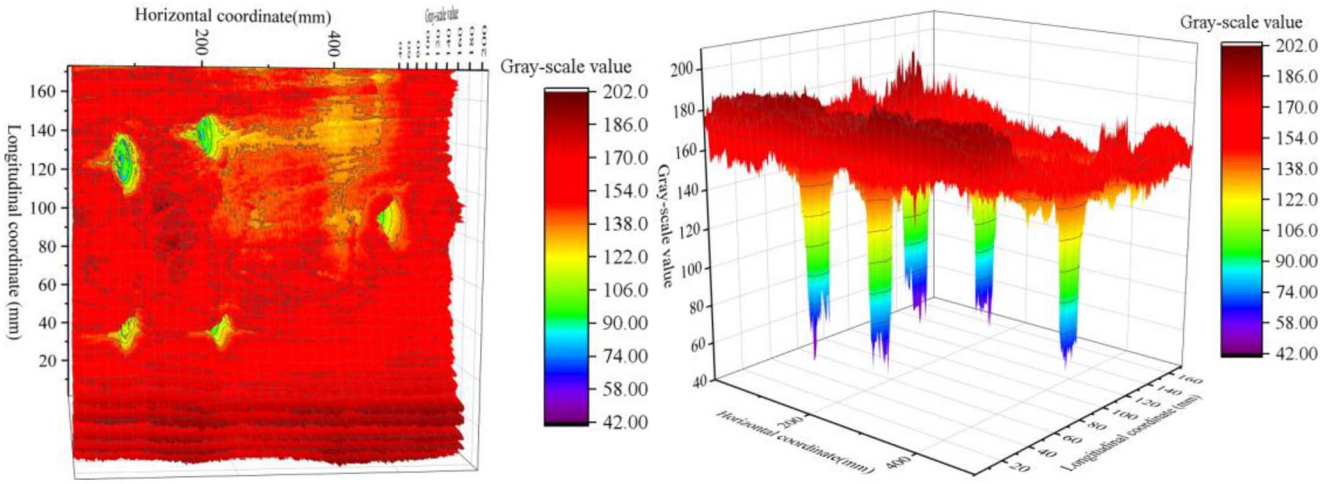

(b)

（c）

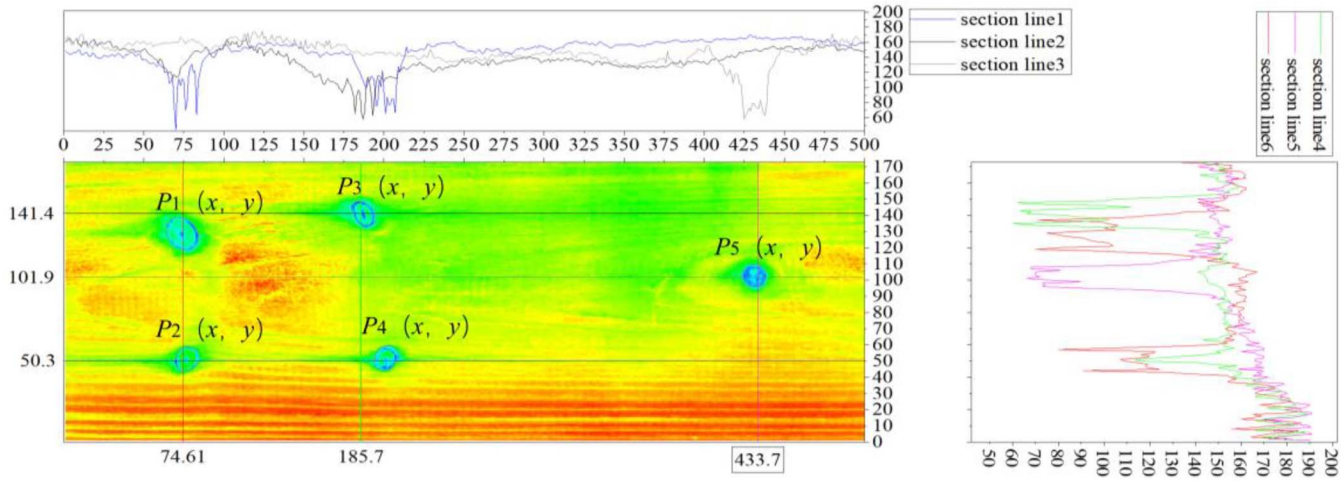

(d)

Figure 18.—Researching and localization of knot areas on structural lumber surfaces: (a) Fujian Chinese fir constructional lumber, (b) contour three-dimensional (3D) mapping curve, (c) projection of 3D mapping curve, and (d) contour sectional graph of knot.

The specific acquisition curve process is as follows: When the sample is tested, a weak signal is generated after it is stressed with the force-measuring sensor, which is amplified by the measuring system and converted by an Analog/Digital converter, and sent to the microcomputer for collection and processing, so as to display the measured load value. Finally, Equations 3 and 4 are used to calculate MOE and modulus of rupture (MOR).

1In the three-point bending test, the load was applied to the wide surface of all sawn timber samples. After applying the load, we show both the sawn timber changes on the applied load surface and the sawn timber changes on the narrow side in Figures 16 and 17.

According to the data measured in the experiment, the corresponding MOE and bending strength is calculated by using Equations 3 and 4, and the difference of the results is analyzed.

$$MOE = \Delta PL^3/(4bh^3\Delta y) \quad (15)$$

$$MOR = 3P_{max}L/(2bh^2) \quad (16)$$

where L is the span, b is the width of the specimen, h is the height of the specimen, y is the stress-strain diagram value, P is the load for which stress-strain diagram y is produced. P_{max} is the breaking load.

Results and Discussion

Evaluation of knots searching and localization

The algorithm can differentiate the knots from the timber background, lower the FCF CL knot-edge detection error, speed up image processing, resist the impact of the surrounding environment to the captured object, and satisfy high-speed and wide-area testing requirements. This study finished the knot localization test on the lumber's surface, verified the precision of the detection model's search and localization, and evaluated the effects of knot on lumber in more detail. In order to aid in the evaluation and grading of the FCF CL, this research will propose an algorithm based on the contour line localization of the gray value of lumber. This method was used for online nondestructive lumber knot detection. The researched knot gray contour change rule also serves as a reference for the detection of other kinds of defects through the use of this method. The knots were searched based on the types and characteristics of FCF CL knots, as well as the gray change curve and contour-fitting diagram created by the gray value contour fitting and extraction method. The calculation results of knot distribution are shown in Figure 18.

The knot localization detection method was used on a 1,000 by 346-mm piece of timber with five knots on its surface, as depicted in Figure 12. Three section lines (x = 74.61 mm, x = 185.7 mm, x = 433.7 mm, y = 50.3 mm, y = 101.9 mm, y = 141.4 mm) were constructed in the transverse and longitudinal directions, respectively, in the contour-fitting diagram. There is a trough and a minimum value for the horizontal section line y = 50.3 mm (section line 1) between x = 70 to 80 mm and x = 200 to 210 mm. To find the position coordinates $P_2(x,y)$ and $P_4(x,y)$ of the knots on the timber, the horizontal section line y = 101.9 mm (section line 3) has a trough within the range of x = 420 to 435 mm and a minimum value. Search and locate the position coordinate $P_5(x,y)$ of the knots on the lumber. The horizontal section line y = 141.4 mm (section line 2) has a trough in the range of x = 175 to 200 mm, and the minimum value appears. Search and locate the position to obtain the position coordinate $P_3(x,y)$ of the knot. The vertical section line x = 74.6 mm (section line 6) has a trough and a minimum value in the range of x = 40-60 mm and x = 120-140 mm. Search and locate the position coordinates $P_2(x,y)$ and $P_3(x,y)$ of the knot. The vertical section line x = 185.7 mm (section line 4) has a trough within the range of x = 135 to 150 mm and a minimum value. Search and locate the position coordinate $P_3(x,y)$ of the knot. The vertical section line x = 433.7 mm (section line 5) has a trough within the range of x = 90 to 110 mm and a minimum value. Search and locate the position coordinate $P_5(x,y)$ of the knot.

Table 3.—The boundary point vector.

Boundary point vector	x coordinate calculation	y coordinate calculation
0	x = x + 1	invariant
1	x = x + 1	y = y − 1
2	invariant	y = y − 1
3	x = x − 1	y = y − 1
4	x = x − 1	invariant
5	x = x − 1	y = y + 1
6	invariant	y = y + 1
7	x = x + 1	y = y + 1

Table 4.—Evaluation of knot positioning accuracy of Fujian Chinese fir constructional lumber.

Position	x (mm)	rBias (%)	rRMSE (%)	Y (mm)	rBias (%)	rRMSE (%)
P_1	65.1	0.61	0.28	109.5	0.42	0.35
P_2	70.3	0.42	0.21	44.8	0.67	0.21
P_3	178.8	0.17	0.21	135.2	0.30	0.28
P_4	193.1	0.16	0.21	45.2	0.84	0.28
P_5	424.6	0.17	0.49	104.5	0.11	0.07

The obvious change of gray-scale value gradient was found at the knot's position, which can accurately locate the knots. Through the steps (the pixel weight calculation on the graph variable edge, spread of the connected domain within the knot, external expansion and internal contraction), the lumber can be effectively analyzed, so as to lay a good foundation for accurate positioning of knots. According to the obtained position information of the knots, the knot distribution of the whole lumber can be further counted, as shown in Table 3. The rBias measured at position x of knots is within 0.61 percent, and the rRMSE(Relative Root Mean Square Error) is within 0.49 percent; the rBias and rRMSE measured at position y of knots are within 0.84 and 0.35 percent (Table 4). The detection results of the three kinds of knots are shown in the Table 5. Based on the machine-vision detection method, the detection time of each piece of sawn timber is 2.2 seconds. Compared with the manual measurenment, the machine-vision detection method for large-size lumber has a relatively high localization detection precision and speed.

Statistics of knot areas

Test sample groups FJS1 through FJS8, with the size of 1,000 by 346 mm, were used to carry out the experiment of searching and locating the knots, as shown in Table 3, and make statistics on the number and positions of knots in

Table 5.—Detection results of different types of knot defects.

Detection type	Detection rate
Dead knot	96.3%
Round knot	94.8%
Edge knot	95.9%

Table 6.—Comparison of defect detection accuracy of different methods.[a]

Method	Machine-vision detection method	Manual measurement
rBias measured at position x	0.61%	Subjective judgment, did not complete the exact location information
rRMSE measured at position x	0.49%	
rBias measured at position y	0.84%	
rBias measured at position y	0.35%	
Measurement time (s)	2.2 s	600 s

[a] The actual data of the lumber measured using a steel tape (accuracy of 1 mm), triangle ruler (accuracy of 1 mm) and a vernier caliper (accuracy of 0.01 mm) was taken as the reference standard value.

lumber. This research method can quickly, simply, and accurately locate and calculate the number and position of knots on the surface of lumber, instead of relying on manual measurement to obtain the information needed for processing and production. Through the observation and application in the production experiment, the growth defects of FCF are mainly knots, which not only affect the wood quality, but also decrease value and reduce the strength or durability of lumber. Knots are located in different positions of lumber, and their influence on the structural properties of dimension is also different from the application mode of building materials. Therefore, after searching and locating the knots, it is of great significance to know size and location of knots. The detection experiment of this sample group shows that, as shown in Table 6, the average number of knots in FJS1 through FJS8, includes two end knots, two knots on the side (0 to 1/4 width and 3/4 width from the origin) and four knots at the center (1/4 to 3/4 width from the origin). The test results of this sample group show that, as shown in Table 7, the proportion of knots at the center (1/4 to 3/4 width from the origin) is relatively high, accounting for 53.33 percent, the proportion of knots on the side (0 to 1/4 width and 3/4 width from the origin) is the second, accounting for 26.67 percent, and the proportion of knots at the center (1/4 to 3/4 width from the origin) is 20.00 percent. The above detection and statistical data show that this method can accurately search and locate knots, which can not only be used as an important basis for the quality evaluation of FCF CL in the later stage. It is also an important step in the production and processing of lumber, breaking the traditional thinking and processing mode of manual visual marking of FCF, and making up for the shortcomings of traditional methods and promoting the safe and stable green application and development of building materials.

Effect of knots on bending resistance of FCF CL

From the appearance, there are many knots in FCF, and most of them are slipknots, with fewer dead knots. The MOE values of six groups of FCF with different knots are 6.11, 6.09, 6.29, 6.39, 6.92, and 6.17 Gpa. The bending strengths of six groups of FCF with different knots are 84.12, 111.99, 107.68, 105.62, 99.69, and 92.07 MPa, and the coefficients of variation are 23, 22, 21, 13, and 21 percent, which are all higher than 15 percent coefficient of variation of bending strength stipulated in the code, as shown in Table 8. The results show that the bending strength of the lumber is good, and there is a correlation between knots and the bending strength of lumber with knots.

It can be seen from Figure 19 that when FCL with knots was pressed from the narrow side, the specimen failure occurred at the knots, and the specimen exhibited stratification and fracture. After the pressure was removed, the specimen showed obvious deformation. Different knot positions will cause different stress distributions, which will change the elastic modulus and bending strength of lumber. When the knot appears on the edge of the FCF CL, it first breaks in the mechanical testing machine, as shown in Figure 20.

In terms of the failure forms of specimens, the failure of FCF was accompanied by slippage and stratification in addition to the fracture of wood fiber. The shape variable of FCF was more obvious after the pressure was removed, especially at knots on the side. The effects of knots of the whole lumber on the strength reducing characteristic were studied to verify that they reduce its load bearing capacity. The study on the effects of knots on the strength-reducing characteristics of FCF CL has verified that knots will reduce its load-bearing capacity.

Based on the developed algorithm, the knots of FCF CL were located, and the weak parts of lumber were searched and determined. Through mechanical bending resistance test, MOE and MOR were determined to study the influence

Table 7.—Position and quantity statistics of knots of Fujian Chinese Fir construction lumber.

Samples	Sum of knots	End knots (pcs.)	Knots on the side 0–1/4 width and 3/ width from the origin (pieces)	Knots at the center 1–3/4 width from the origin (pieces)
FJS1	7	3	1	3
FJS2	5	1	1	3
FJS3	9	2	1	6
FJS4	12	2	6	4
FJS5	5	2	0	3
FJS6	8	2	1	5
FJS7	8	0	3	5
FJS8	6	0	3	3
sum	60	12	16	32
average	7.5	1.5	2	4

Table 8.—The proportion statistics of the position and number of knots of Fujian Chinese Fir constructional lumber.

Samples	End knots proportion (%)	Knot proportion on the side 0–1/4 width and 3/4 width from the origin (%)	Knot proportion at the center 1–3/4 width from the origin (%)
FJS1	42.86	14.29	42.86
FJS2	20.00	20.00	60.00
FJS3	22.22	11.11	66.67
FJS4	16.67	50.00	33.33
FJS5	40.00	0.00	60.00
FJS6	25.00	12.50	62.50
FJS7	0.00	37.50	62.50
FJS8	0.00	50.00	50.00
Average	20.00	26.67	53.33

of knots on mechanical properties of FCF CL. As shown in Table 9, knots will reduce the mechanical properties of FCF CL. The MOE average decline rate of knotted FCF is 2.40 percent. The bending strength of FCF with knots is good, and there is a significant correlation between knots and the bending strength of CL with knots. The MOR average decline rate of knotted FCF is 29.17 percent. Knots will reduce the bending strength of lumber, especially knots at the edge (FJ-S-G). In the area with knots, the average MOE and MOR of CL are 6.33 GPA and 100.20 MPa respectively. The above research shows that the mechanical properties of FCF CL are gradually reduced by the knots. Knots are the main defect characteristic of FCF CL. Knots are an important factor affecting MOE and MOR of lumber. They lay a foundation for the study of various defects affecting strength or related properties on the surface of lumber.

Conclusions

Defect searching and FCF CL localization are the primary focus of this work. Combining image processing with the surface characteristics of FCF CL, a practical and effective approach for locating knots in FCF CL was presented. The approach satisfies the requirements of large-area lumber testing while mitigating the impact of the environment on the captured object. We analyzed and processed the gray value of the knot region and non-knot area of CL using FCF anisotropy and knot gray features. The knots' contour misfitting issues were resolved, and loss of edge information successfully prevented. By extracting knot characteristics, position detection accuracy was improved. A wave trough emerged in the profile line during the gradient shift of the gray value contour line, fitting the knots' outlines. This algorithm is used to obtain the knots' positions and subsequently count the knot distribution across the lumber. This kind of nondestructive testing is used to examine the mechanical properties of FCF CL. By using contour-fitting and extraction algorithms to locate knots, grading can be made more accurate and efficient, increasing the amount of wood utilized and its application to real production.

Future Research Possibilities

In future research work, the technology of machine-vision technology can be combined with other sawn timber identification technologies, such as ultrasonic detection, X-ray detection technology, or infrared thermal image detection, to determine whether there are defects inside the wood, to detect and locate the defects of sawn timber, and to improve the accuracy of the prediction of sawn timber mechanical properties.

There are various options for sawn timber machine-vision surface defect recognition technology such as manual visual inspection, machine-vision technology, and deep learning technology. Each technology has its advantages and limitations, and users can choose the appropriate technology according to their own needs and conditions. In the future, with the continuous development of science and technology, these technologies may be further improved and perfected, bringing more possibilities for sawn timber inspection.

With increasing environmental awareness and the promotion of green building, more and more buildings are using timber as the main building material. This not only raises

Figure 19.—Cracks in the final failure of Fujian Chinese fir (with knots): (a) test sample of FCF:FJ-S-G13, (b) test sample of FCF: FJ-S-G15, and (c) test sample of FCF:FJ-S-G16.

S-G15 (c) test sample of FCF:FJ-S-G16

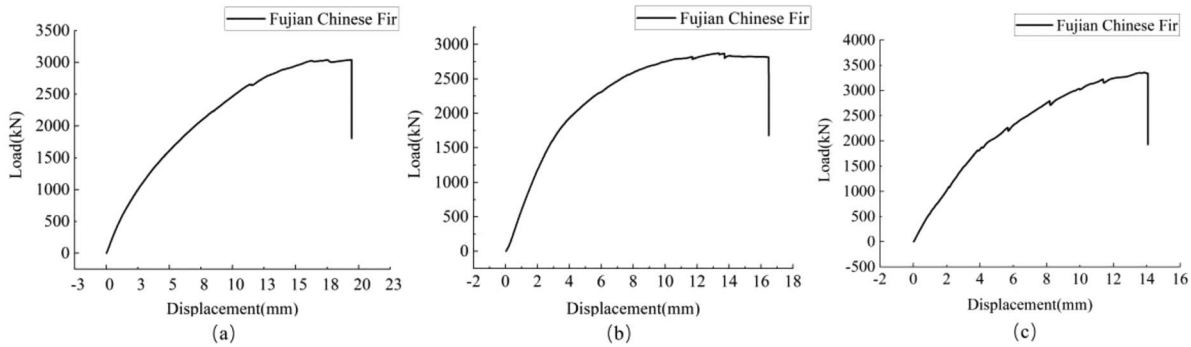

Figure 20.—Displacement-load curves of several typical Fujian Chinese fir with knots: (a) FJ-S-G13, (b) FJ-S-F15, and (c) FJ-S-G15.

Table 9.—Effect of knots on bending resistance of Fujian Chinese Fir constructional lumber.

Groups	MOE (GPa)[a] ± SE	MOR (MPa) ± SE
A	6.11 ± 0.87	84.12 ± 7.05
E	6.09 ± 1.78	111.99 ± 25.33
F	6.29 ± 2.27	107.68 ± 16.21
G	6.39 ± 2.51	105.62 ± 21.78
H	6.92 ± 1.71	99.69 ± 12.63
T	6.17 ± 1.54	92.07 ± 19.76

A MOE = modulus of elasticity; MOR = modulus of rupture.

the demand for timber, but also puts higher requirements on the quality of timber. Therefore, how to improve the quality of sawn timber so that it can better meet the needs of building materials, furniture production and other needs will be an important direction for the future work of sawn timber grading and so on.

With the development of big data and cloud computing technologies, in particular the advancement of artificial intelligence and machine-vision technologies, sawn timber preference technologies are expected to be further optimized to achieve higher precision and automated timber selection and classification. For example, sawn timber can be scanned and analyzed quickly and accurately by machine-vision technology, and then algorithms can be used to accurately assess the quality, dimensions, and other information of the sawn timber to achieve automatic grading of the sawn timber.

Wood can also be used in shipbuilding, aerospace, and other fields, with the advantages of light weight, fire prevention, environmental protection, and so on. With the development of science and technology, people are constantly innovating and expanding the way they utilize wood. The technology of grading sawn timber is expected to become more precise, fast, and automated, as well as to better meet the application of timber materials in different fields, in order to adapt to the trend of sustainable development in the future.

Table 10.—Modulusl of elasticity (MOE) and modulus of rupture (MOR) decline rates of knotted Fujian Chinese fir.

Samples	MOE (GPa)	MOR (MPa)
FJ-S-G12	0.8%	35%
FJ-S-G13	0.9%	33%
FJ-S-G14	1.8%	30%
FJ-S-F15	2.5%	28%
FJ-S-G16	4.1%	26%
FJ-S-G17	4.3%	23%

Acknowledgments

This work was supported by Program of Fujian Provincial Science and Technology Programme for External Cooperation Project(Grant No. 2023I1012), Fujian Provincial Science and Technology Programme Project Central Guiding Local Science and Technology Development Special Project (Grant No. 2022L3063), Forestry Science and Technology Promotion Project of State Forestry and Grassland Administration of China (Grant No. (2019)35), National Natural Science Foundation of China (CN) (Grant No. 31670721).

Literature Cited

Ahn, J., J. Lee, and K. Hong. 2021. Genetic diversity and structure of Pinus densiflora Siebold & Zucc. populations in Republic of Korea based on microsatellite markers. *Forests* 12(6):750−764. https://doi.org/10.3390/f12060750

Ashok, K. P., N. M. Venkata, K. A. Dinesh, and R. N. Soumya. 2021. Surface defect detection using SVM-based machine vision system with optimized feature. *Machine Vis. Inspect. Syst*. 2:109−127. https://doi.org/10.1002/9781119786122.ch6

Blokland, J. V, V. Nasir, J. Cool, S. Avramidis, and S. Adamopoulos. 2021. Machine learning-based prediction of surface checks and bending properties in weathered thermally modified timber. *Construct. Building Mater*. 307:124996. https://doi.org/10.1016/j.conbuildmat.2021.124996

Brunetti, M., P. Burato, C. Cremonini, F. Negro, M. Nocetti, and R. Zanuttini. 2016. Visual and machine grading of larch (Larix decidua Mill.) structural timber from the Italian Alps. *Mater. Struct*. 49(7):2681−2688. https://doi.org/10.1617/s11527-015-0676-5

Burawska-Kupniewska, I., S. Krzosek, and P. Mankowski. 2021. Efficiency of visual and machine strength grading of sawn timber with respect to log type. *Forests* 12(11):1467. https://doi.org/10.3390/f12111467

Castellanos, F. J., A.-J. Gallego, and J. Calvo-Zaragoza. 2021. Unsupervised neural domain adaptation for document image binarization. *Pattern Recogn*. 119:108099, https://doi.org/10.1016/j.patcog.2021.108099

Chang, S. L., M. C. Young, L. Hansol, H. P. Jung, and H. L. Chi. 2018. Establishment, regeneration, and succession of Korean red pine (Pinus densiflora S. et Z.) forest in Korea. Ana Cristina Gonçalves, In: Conifers. IntechOpen, London, UK. pp. 47−76. https://doi.org/10.5772/intechopen.80236

Damme, M. 2021. A process-based method for predicting lateral erosion rates. *Nat. Hazards* 107:375–394. https://doi.org/10.1007/s11069-021-04587-y

Devaru, D. G. and B. Gopalakrishnan. 2020. Regression model to estimate the electrical energy consumption of lumber sawing based on the product, process, and system parameters. *Energy Efficiency* 13:1799–1824. https://doi.org/10.1007/s12053-020-09907-y

Gao, H., M. Hua, T. Gao, and R. Cheng. 2019. Robust detection of median filtering based on combined features of difference image. Signal Process. *Image Commun*. 72:126–133. https://doi.org/10.1016/j.image.2018.12.014

Gu, Y. H., H. Andersson, and R. Vicen. 2010. Wood defect classification based on image analysis and support vector machines. *Wood Sci. Technol*. 44(4):693–704. https://doi.org/10.1007/s00226-009-0287-9

Hyun, J. S., K. K. Nam, M. J. Jeong, and C. L. Min. 2018. Fire properties of Pinus densiflora utilizing fire-retardant chemicals based on borate and phosphorus (II)—Thermal and gas emission characteristics. *Bio Resources* 13(1):5417–5427. https://doi.org/10.1016/j.image.2018.12.014

The European Standard EN 13183-1:2002 has the status of a British Standard. Moisture content of a piece of sawn timber Part 2: Estimation by electrical resistance method.

Jenkel, C. and M. Kaliske. 2018. Simulation of failure in timber with structural inhomogeneities using an automated FE analysis. *Comput. Struct*. 207:19–36. https://doi.org/10.1016/j.compstruc.2017.11.016

Kamal, K., R. Qayyum, S. Mathavan, and T. Zafar. 2017. Wood defects classification using laws texture energy measures and supervised learning approach. *Adv. Eng. Inform*. 34:125–135. https://doi.org/10.1016/j.aei.2017.09.007

Kandler, G., M. Lukacevic, and Josef Füssl. 2016. An algorithm for the geometric reconstruction of knots within timber boards based on fibre angle measurements Construct. *Building Mater*. 124:945–960. http://dx.doi.org/10.1016/j.conbuildmat.2016.08.001

Kang, H., B. Seely, G. Wang, Y. Cai, J. Innes, D. Zheng, P. Chen, and T. Wang. 2017. Simulating the impact of climate change on the growth of Chinese fir plantations in Fujian province, China. *N. Z. J. Forestry Sci*. 47:20. https://doi.org/10.1186/s40490-017-0102-6

Kopp, W., R. Monti, A. Tamburrini, U. Ohler, and A. Akalin. 2020. Deep learning for genomics using Janggu. *Nat. Commun*. 11:3488. https://doi.org/10.1038/s41467-020-17155-y

Li, X., F. Zhou, H. Tan, W. Zhang, and C. Zhao. 2021. Multimodal medical image fusion based on joint bilateral filter and local gradient energy. *Inf. Sci*. 569:302–325. https://doi.org/10.1016/j.ins.2021.04.052

Longo, B. L., F. Brüchert, G. Becker, and U. H. Sauter. 2019. Validation of a CT knot detectionalgorithm on fresh Douglas-fir (Pseudotsuga menziesii (Mirb.) Franco) logs. *Ann. Forest Sci.* 76(2):28. https://doi.org/10.1007/s13595-019-0812-4

Lukacevic, M., G.g Kandler, M. Hu, A.rs Olsson, and J.sef Füssl. 2019. A 3D model for knots and related fiber deviations in sawn timber for prediction of mechanical properties of boards. *Mater. Des*. 166:107617. https://doi.org/10.1016/j.matdes.2019.107617

Ma, S., K. Ashraf, H. Hassan, and E. Hichem. 2020. Quantum dilation and erosion. *Appl. Sci*. 10(11):4040. https://doi.org/10.3390/app10114040

Mahram, A., M. G. Shayesteh, and S. Jafarpour. 2012. Classification of wood surface defects with hybrid usage of statistical and textural features. In: 2012 35th International Conference on Telecommunications and Signal Processing (TSP). 03-04 July 2012, Prague, Czech Republic, IEEE. pp. 749–752. doi: 10.1109/TSP.2012.6256397

National standard of the People's Republic of China, GB/T 50329-2012 Standard for test methods of timber structures.

National standard of the People's Republic of China, GB/T 1936.1-2009 Method of testing in bending strength of wood.

Panagiotis, B., D. Kosmas, B. Ioannis, G. Nikos, and L. Panagiotis. 2018. Wood species recognition through multidimensional texture analysis. *Comput. Electron. Agric*. 144:241–248. https://doi.org/10.1016/j.compag.2017.12.011

Pahlberg, T., O. Hagman, and M. Thurley. 2015. Recognition of boards using wood fingerprints based on a fusion of feature detection methods. *Comp. Electron. Agric*. 111:164–173.

Pan, S., S. Fan, S. W. K. Wong, V. Z. James, and R. Helge. 2021. Ellipse detection and localization with applications to knots in sawn lumber images. In: Proceedings of the IEEE/CVF Winter Conference on Applications of Computer Vision (WACV). 03-08 January 2021, IEEE, Waikoloa, HI, USA, pp. 3892–3901. doi:10.1109/WACV48630.2021.00394

Pang, G., C. Shen, L. Cao, and V. D. H. Anton. 2021. Deep learning for anomaly detection: A review. *ACM Comput. Surv*. 54(2):1–38. https://doi.org/10.1145/3439950

Panwar, H., P. K. Gupta, M. K. Siddiqui, R. M. Menendez, and V. Singh. 2020. Application of deep learning for fast detection of COVID-19 in x-rays using nCOVnet. *Chaos Solitons Fractals* 138:109944. https://doi.org/10.1016/j.chaos.2020.109944

Park, J., W. Kim, W. Kim, C. Park, C. Y. Choi, J. Cho, S. Kim, and H. Cheong. 2021. Antihypertensive effects of dehydroabietic and 4-epi-transcommunic acid isolated from Pinus densiflora. *J. Med. Food* 24(1):50–58. https://doi.org/10.1089/jmf.2020.4797

Qiu, Q., R. Qin, J. H. M. Lam, A. M. C. Tang, M. W. K. Leung, and D. Lau. 2019. An innovative tomographic technique integrated with acoustic-laser approach for detecting defects in tree trunk. *Comput. Electron. Agric*. 156:129–137. https://doi.org/10.1016/j.compag.2018.11.017

Ramage, M. H., H. Burridge, M. Busse-Wicher, G. Fereday, T. Reynolds, D. U. Shah, G. Wu, L. Yu, P. Fleming, D. Densley-Tingley, J. Allwood, P. Dupree, P. F. Linden, and O. Scherman. 2017. The wood from the trees: The use of timber in construction. Renew. *Sustain. Energy Rev*. 68:333–359. https://doi.org/10.1016/j.rser.2016.09.107

Shuaeb, S. M. A. A., M. Kamruzzaman, and M. H. Ali. 2021. Extracting a bounded region from a map using flood fill algorithm. *Asian J. Res. Comput. Sci*. 7(1):14–20. https://doi.org/10.9734/ajrcos/2021/v7i130170

Singh, K., B. Sharma, J. Singh, G. Srivastava, S. Sharma, A. Aggarwal, and X. Cheng. 2020. Local statistics-based speckle reducing bilateral filter for medical ultrasound images. *Mobile Netw. Appl*. 25:2367–2389. https://doi.org/10.1007/s11036-020-01615-2

Su, X., S. Li, X. Wan, Z. Huang, B. Liu, S. Fu, P. Kumar, and Y. H. C. Han. 2021. Understory vegetation dynamics of Chinese fir plantations and natural secondary forests in subtropical China. *Forest Ecol. Manag*. 483(1):118750. https://doi.org/10.1016/j.foreco.2020.118750

Tang, H., R. Ni, Y. Xiao, and L. Li. 2018. Median filtering detection of small-size image based on CNN. *J. Vis. Commun. Image Represent*. 51:162–168. https://doi.org/10.1016/j.jvcir.2018.01.011

Tian, Y., B. Wu, X. Su, Y. Qi, Y. Chen, and Z. Min. 2021. A crown contour envelope model of Chinese fir based on random forest and mathematical modeling. *Forests* 12(1):48. https://doi.org/10.3390/f12010048

Tu, Y., Z. Ling, S. Guo, and H. Wen. 2021.An accurate and real-time surface defects detection method for sawn lumber. *IEEE Transact. Instrum. Meas*. 70:1–11. https://doi.org/10.1109/TIM.2020.3024431

Valle, M. E. 2020. Reduced dilation-erosion perceptron for binary classification. *Mathematics* 8(4):512. https://doi.org/10.3390/math8040512

Viguier, J., D. Bourreau, J. F. Bocquet, G. Pot, L. Bléron, and J. Lanvin. 2017. Modelling mechanical properties of spruce and Douglas fir timber by means of X-ray and grain angle measurements for strength grading purpose. *Eur. J. Wood Prod*. 75:527–541. https://doi.org/10.1007/s00107-016-1149-4

Viguier, J., A. Jehl, R. Collet, L. Bleron, and F. Meriaudeau. 2015. Improving strength grading of timber by grain angle measurement and mechanical modeling. *Wood Mater. Sci. Eng*. 10(1):145–156. https://doi.org/10.1080/17480272.2014.951071

Wang, G., J. C. Ye, and B. De Man. 2020a. Deep learning for tomographic image reconstruction. *Nat. Machine Intell*. 2:737–748. https://doi.org/10.1038/s42256-020-00273-z

Wang, J., X. Wang, Q. He, Y. Zhang, and T. Zhan. 2020b. Time-temperature-stress equivalence in compressive creep response of Chinese fir at high-temperature range. *Construct. Building Mater*. 235:117809. https://doi.org/10.1016/j.conbuildmat.2019.117809

Wright, S., J. Dahlen, C. Montes, and T. L. Eberhardt. 2019. Quantifying knots by image analysis and modeling their effects on the mechanical properties of loblolly pine lumber. *Eur. J. Wood Prod.* 77:903–917. https://doi.org/10.1007/s00107-019-01441-8

Yang, J., H. Ren, G. Zhu, J. Huang, and Y. Shi. 2018. Detecting median filtering via two-dimensional AR models of multiple filtered residuals. *Multimedia Tools Appl*. 77:7931–7953. https://doi.org/10.1007/s11042-017-4691-0

Yu, H., F. He, and Y. Pan. 2020. A scalable region-based level set method using adaptive bilateral filter for noisy image segmentation. *Multimed Tools Appl*. 79:5743–5765. https://doi.org/10.1007/s11042-019-08493-1.

Yuan, Q., H. Shen, T. Li, Z. Li, S. Li, Y. Jiang, H. Xu, W. Tan, Q. Yang, J. Wang, J. Gao, and L. Zhang. 2020. Deep learning in environmental remote sensing: Achievements and challenges. *Remote Sens. Environ*. 241:111716. https://doi.org/10.1016/j.rse.2020.111716

Yue, K., Z. Chen, W. Lu, W. Liu, M. Li, Y. Shao, L. Tang, and L. Wan. 2017. Evaluating the mechanical and fire-resistance properties of modified fast-growing Chinese fir timber with boric-phenol-formaldehyde resin. *Construct. Building Mater*. 154:956–962. https://doi.org/10.1016/j.conbuildmat.2017.08.035

Yue, K., J. Wu, L. Xu, Z. Tang, Z. Chen, W. Liu, and L. Wang. 2020. Use impregnation and densification to improve mechanical properties and combustion performance of Chinese fir. *Construct. Building Mater*. 241(30):118101. https://doi.org/10.1016/j.conbuildmat.2020.118101

Zhan, T., J. Jiang, J. Lu, Y. Zhang, and J. Chang. 2019. Temperature-humidity-time equivalence and relaxation in dynamic viscoelastic response of Chinese fir wood. *Construct. Building Mater*. 227:116637. https://doi.org/10.1016/j.conbuildmat.2019.08.018

Zhang, Y., R. Tong, D. Song, X. Yan, L. Lin, and J. Wu, 2020. Joined fragment segmentation for fractured bones using GPU-accelerated shape-preserving erosion and dilation. *Med. Biol. Eng. Comput*. 58:155–170. https://doi.org/10.1007/s11517-019-02074-y

Zhao, J., M. Meng, Z. Jin, D. Chen, Y. Wu, and W. Zhang. 2019. Bending properties of bamboo scrimber with holes in different sizes and positions. *Construct. Building Mater*. 200:209–217. https://doi.org/10.1016/j.conbuildmat.2018.12.076